



# (La,Sr)(Ti,Ni)O<sub>3</sub> and YSZ Composite Anodes with Impregnated GDC Nanoparticles as Fuel Electrodes for Solid Oxide Fuel Cells

Yao Jiang<sup>1</sup>, Haonan Huang<sup>1</sup>, Mingqing Li<sup>1</sup>, Linxin Zhang<sup>1</sup>, Yabing Diao<sup>1</sup>, Hang Tan<sup>1</sup>, Chami N.K. Patabendige<sup>2</sup>, Cairong Jiang<sup>1,\*</sup>, Jianjun Ma<sup>1,\*</sup>

<sup>1</sup> School of Materials Science and Engineering, Sichuan University of Science and Engineering, Zigong, Sichuan, 643000, PR China

crjiang@suse.edu.cn; jjma@suse.edu.cn

<sup>2</sup> Department of Science for Technology, Faculty of Technology, University of Sri Jayawardenepura, Dampe - Pitipana Rd, Homagama, Sri Lanka

**Abstract.** Titanate anode materials have emerged as a focal point of research in solid oxide fuel cells (SOFCs) due to their high adaptability to diverse fuel gases. To further enhance their performance, we propose an impregnation strategy to create a composite electrode by applying a gadolinium-doped cerium oxide (GDC, Ce<sub>0.9</sub>Gd<sub>0.1</sub>O<sub>2-σ</sub>) solution to a La, Ni co-doped SrTiO<sub>3</sub> (LSTN) anode. This approach aims to improve the effectiveness of the anode material in SOFC applications. The composite anode, which was treated with of GDC 3 impregnation cycles, achieved a polarization resistance of 1.21 Ω cm<sup>2</sup> and a maximum power density of 79.52 mW cm<sup>-2</sup> after being reduced at 800 °C for 2 hours. It was tested at various temperatures and with different amounts of impregnated GDC.

**Keywords:** Impregnation method; Nano-composite electrode; Solid oxide fuel cell.

## 1 Introduction

Strontium titanate (SrTiO<sub>3</sub>) exhibits excellent stability in its perovskite structure, along with notable doping tolerance and resistance to carbon deposition. However, its electrical conductivity and catalytic activity are lower than those of metallic materials. Current research is focused on enhancing electrical conductivity by partially substituting the strontium (Sr) element with lanthanum (La), calcium (Ca), and other elements, as well as by strategically designing A-site defects[1] [2]. Additionally, B-site doping with transition metals such as iron (Fe), cobalt (Co), and nickel (Ni) facilitates the formation of homogeneously dispersed metal nanoparticles through the exsolution process, thereby improving catalytic activity [3].

La-Ni co-doped SrTiO<sub>3</sub> (LSTN) is a promising candidate for a fuel electrode in solid oxide fuel cells[4]. Previous studies have demonstrated that LSTN exhibits exceptionally high electronic conductivity. However, the ionic conductance is often insufficient, which frequently necessitates using Yttria-Stabilized Zirconia (YSZ) or Gadolinium-Doped Ceria (GDC) as composite anodes. Among these, YSZ is a widely utilized electrolyte material. To ensure compatibility between the anode and electrolyte, they must have similar thermal expansion coefficients. The LSTN-YSZ anode is considered one of the ideal composite anode materials.

Choi et al. [5] achieved improved performance by combining LSTN and GDC composite anodes with

scandia-stabilized zirconia (ScSZ) electrolytes. However, this typically necessitates the addition of a GDC overlayer to prevent interfacial reactions between La and Ti in the LSTN anode and Zr and Sc in the ScSZ electrolyte. Horita et al. [6] demonstrated high thermal cycling stability by using GDC impregnated in La-doped SrTiO<sub>3</sub> nanofibres substrates. This solution impregnation of GDC can produce anodes with a microchannel structure characterized by high strength, excellent orientation, significant porosity, and a large specific surface area. These features provide abundant active sites and highly efficient gas transport channels for electrochemical reactions [7, 8].

Herein, the LSTN-YSZ composite anode, composed of (La<sub>0.4</sub>Sr<sub>0.6</sub>)<sub>0.87</sub>Ti<sub>0.95</sub>Ni<sub>0.05</sub>O<sub>3</sub> and YSZ in a mass ratio of 1:1, was evaluated as a structural backbone. Subsequently, a GDC precursor solution was impregnated onto this composite anode. To determine the optimal amount of impregnation, we conducted multiple trials and analyzed the relationship between various test temperatures, reduction times, and impregnation amounts. This investigation focused on the composite anode's phase structure, reduction stability, and electrochemical properties.

## 2 Experimental

The LSTN-YSZ||YSZ||LSM-YSZ cells were prepared following the methodologies outlined in previous studies [7-9]. This preparation involved dissolving analytically pure Gd(NO<sub>3</sub>)<sub>3</sub>·6H<sub>2</sub>O (99%, Sinopharm) and Ce(NO<sub>3</sub>)<sub>3</sub>·6H<sub>2</sub>O (99%, Sinopharm) in deionized water according to a predetermined stoichiometric ratio. An appropriate amount of lemon hexahydrate was then added to create the GDC precursor solution. The preparation of LSTN-YSZ (GDC), YSZ, and LSM-YSZ cells with varying GDC contents was conducted using the impregnation method. For comparison, LSTN-YSZ anodes without any treatment (GDC 0) were prepared using the same process. The anodes were one impregnation cycle for GDC 1) and three impregnation cycles for GDC 3 to obtain composite anodes with different levels of GDC impregnation.

**Table1.** Objects of electrochemical performance analysis.

GDC 0	GDC1	GDC 3
unimpregnated GDC	One impregnation cycle	three impregnation cycles

X-ray diffraction (XRD) patterns (D2 PHASER, Bruker) of the powders were utilized to analyze the physical phase structure of the prepared LSTN, YSZ, and GDC, and qualitatively assess the phase purity of these samples. The surface morphology of the SOFC single cell, LSTN-YSZ sintered body samples, and impregnated LSTN-YSZ composite anode powder samples was examined in detail using a TESCAN-3 scanning electron microscope.

An electrochemical workstation (Solartron 1260A+1287, United Kingdom) was utilized to record the impedance spectra of individual cells with an AC amplitude of 10 mA, spanning a frequency range from 1 MHz to 0.1 Hz.

## 3 Results and discussion

The basic flow of GDC impregnation is illustrated in Fig. 1a. XRD analysis of pristine LSTN, YSZ, and GDC powders (Figs. 1b, 1c, and 1d) revealed that, under the specified preparation conditions, the LSTN powders exhibited a standard cubic perovskite structure. The XRD patterns for LSTN (Fig. 1b,

PDF#04-005-7016), YSZ (Fig. 1c, PDF#96-152-8645), and GDC (Fig. 1d, PDF#97-018-4585) demonstrated that these materials were well-crystallized, with no significant impurity peaks detected. Following impregnation with GDC, the XRD pattern indicates that the LSTN and YSZ matrix remains the primary phase, while significant diffraction peaks corresponding to GDC are also present. This analysis confirms that  $Gd^{3+}$  cations can be homogeneously incorporated into the fluorite lattice of cerium, appearing as GDC at the interface of the composite anode with the LSTN-YSZ matrix[9].

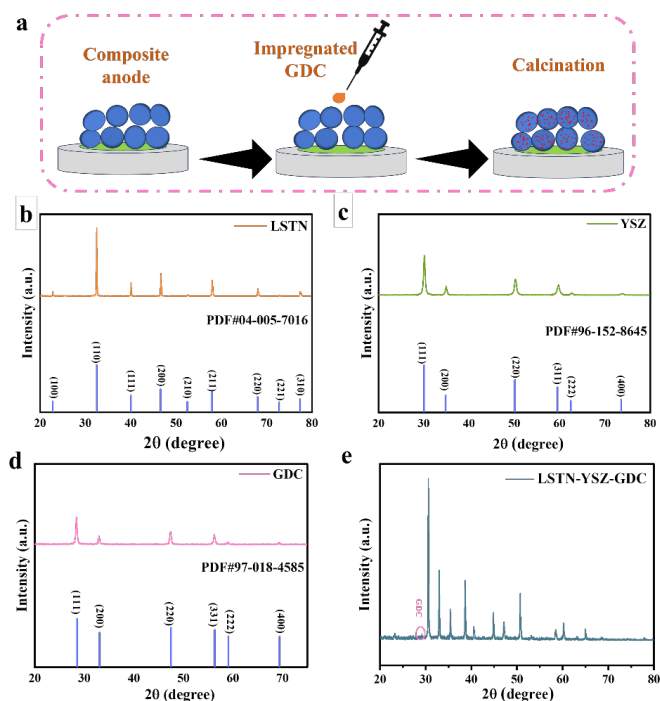


**Fig. 1** a) Schematic diagram of the GDC impregnation process. XRD patterns of b) LSTN powders, c) YSZ powders, d) GDC powders, e) LSTN-YSZ (GDC 3) anode.

GDC was impregnated into the LSTN-YSZ composite anode at 800 °C under humidified hydrogen for electrochemical impedance spectroscopy (EIS) (Fig. 2a) and current-voltage profile testing (I-V-P) (Fig. 2b) to evaluate the electrochemical performance of the cell samples. The ohmic and polarization resistances at the open-circuit voltage (OCV) for the samples without impregnation were 2.84 and 2.57  $\Omega$  cm<sup>2</sup>, respectively. In contrast, the polarization resistance of the samples underwent a single impregnation treatment was 1.40  $\Omega$  cm<sup>2</sup>. Furthermore, for the samples with three impregnation cycles, the polarization resistance decreased to a minimum value of 1.26  $\Omega$  cm<sup>2</sup>. Three types of resistances were identified within the polarization resistance: high-frequency resistor ( $R_1$ ), medium-frequency resistor ( $R_2$ ), and low-frequency resistor ( $R_3$ )[10, 11]. According to the analysis of EIS plot, the majority of the reduced resistance is observed in the  $R_3$  stage. For the GDC-rich composite anode material, the  $R_3$  value is even smaller, indicating improved adsorption and conversion processes for oxygen ions in the composites after GDC impregnation. This demonstrates that GDC impregnation enhances the transfer of oxygen ions to the composite anode. Additionally, the ohmic resistances were measured as follows: 2.84  $\Omega$  cm<sup>2</sup> for GDC 0, 2.74  $\Omega$  cm<sup>2</sup> for GDC 1, and 2.58  $\Omega$  cm<sup>2</sup> for GDC 3, showing a gradual decrease with

an increasing number of impregnation cycles. Ohmic resistance primarily arises from the combination of electrolyte, electrode, and electrode-electrolyte contact resistance. Since the same electrolyte was used for all samples in this study, it indicates that GDC impregnation contributes to reducing the ohmic resistance of the composite electrode itself, with resistance decreasing progressively as the number of GDC impregnation cycles increases. The values for the EIS at different test temperatures are presented in Fig. 2c. The data indicate that both polarization resistance and ohmic resistance tend to decrease with an increasing number of impregnation cycles across test temperatures ranging from 700 to 800 °C.

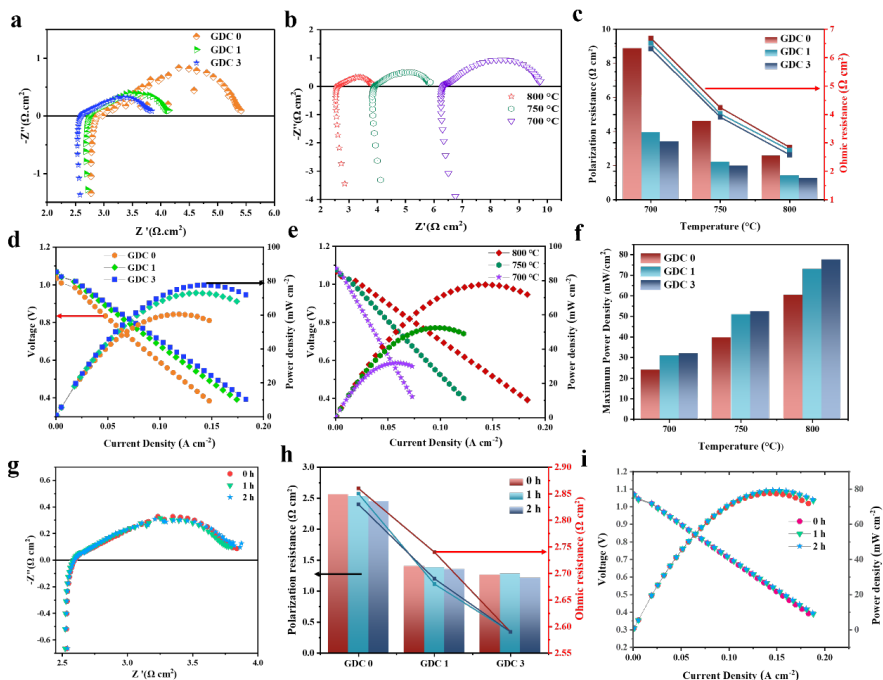


**Fig. 2.** Performance for SOFC with different impregnation cycles. a) EIS curves of cells with different GDC impregnation cycles; b) EIS of the GDC3 cell tested at different test temperatures. c) Comparison of polarization resistance and ohmic resistance of samples with different impregnation cycles; d) I-V-P curves of cells with different GDC impregnation cycles; e) I-V-P curves of the GDC3 cell at different test temperatures; f) Comparison of the maximum power density with different impregnation cycles; g) EIS curves of cells with different reduction time. h) Plot of polarization and ohmic resistance with different reduction time and impregnation cycles. i) I-V-P curves of cells with different reduction time.

Figure 2d illustrates the results of SOFC tests conducted with varying numbers of impregnation cycles. The OCV consistently ranges from -1.06 V to -1.07 V, aligning with the theoretical open-circuit voltage range and indicating that there was no gas leakage during the tests. The observed linear relationship between voltage and current density, as current density increases, suggests that there are no significant barriers to the process of activation polarization, concentration polarization, and ohmic polarization. However, there are notable differences in maximum power density among the samples, with values recorded at 60.43 mW cm<sup>-2</sup> for GDC 0, 73.01 mW cm<sup>-2</sup> for GDC 1, and 77.62 mW cm<sup>-2</sup> for GDC 3 for the three samples. The differences in power density between the unimpregnated samples and those impregnated once and three impregnation cycles were 13 mW cm<sup>-2</sup> and 17 mW cm<sup>-2</sup>, respectively.

Furthermore, the performance of the GDC 3 at different temperatures is presented in Fig. 2e. The maximum power densities recorded were  $77.62 \text{ mW cm}^{-2}$  at  $800 \text{ }^\circ\text{C}$ ,  $52.40 \text{ mW cm}^{-2}$  at  $750 \text{ }^\circ\text{C}$ , and  $31.94 \text{ mW cm}^{-2}$  at  $700 \text{ }^\circ\text{C}$ . This indicates that the cells with surface-impregnated GDC maintained stability across various test temperatures and exhibited superior performance. Fig. 2f displays the maximum power density for different numbers of impregnation cycles at varying temperatures, demonstrating that GDC 3 consistently outperforms the others across the temperature ranges tested.

Reduction at  $800 \text{ }^\circ\text{C}$  for varying durations is a crucial method for characterizing the stability of GDC materials. Figures 2g, 2h, and 2i illustrate the electrochemical properties at  $800 \text{ }^\circ\text{C}$  under humidified hydrogen ( $\text{H}_2$ ) for different time intervals. The results indicate a slight improvement in electrochemical performance after 1 hour, while the EIS and I-V-P curves for the 2-hour and 1-hour test are nearly coincident. This observation may be attributed to a modest enhancement in the catalytic performance of the cell, possibly due to the in-situ exsolution of nickel when maintained at  $800 \text{ }^\circ\text{C}$  for 1 hour. This demonstrates that composite anodes containing both impregnated and unimpregnated GDC can still exhibit a linear relationship between voltage and current as the current density increases, with the polarization resistance remaining nearly constant.

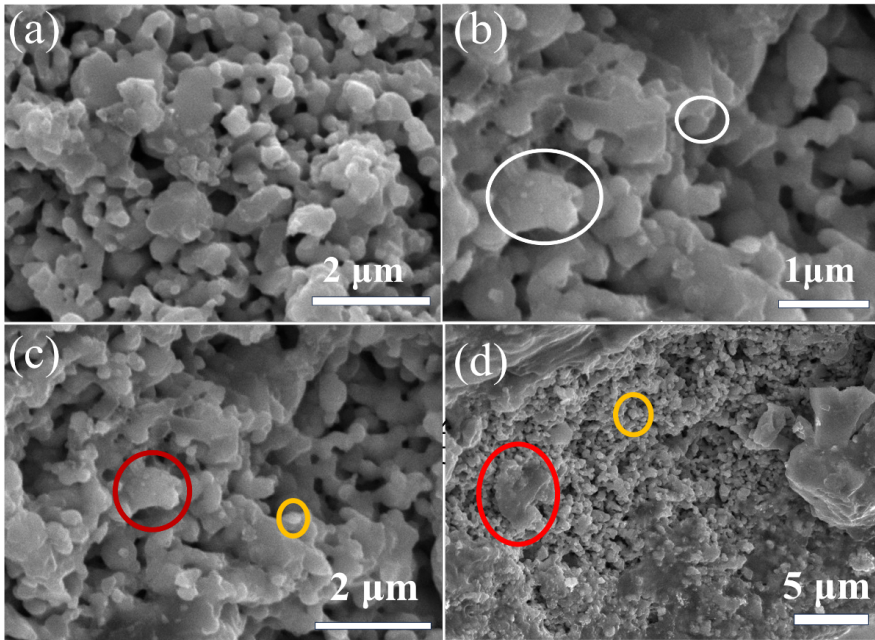


**Fig. 3.** Morphological analysis. (a) for unimpregnated anodes, and (b) for anodes impregnated with 3 impregnation cycles. (c) and (d) are anodes impregnated with 3 impregnation cycles at different magnifications.

Figure 3 shows the scanning electron microscope images of the anode of the unimpregnated GDC (Fig. 3(a)) and the anode of the sample impregnated with 3 impregnation cycles of GDC (Fig. 3(b)), as well as the anode of the sample, at low and high magnifications. Nanoparticles GDC were formed on the LSTN composite anode using impregnation treatment, as shown in the circled image in Fig. 3(b). According to Fig. 3c and d, the YSZ (orange circles) and LSTN (red circles) layers are homogeneous and well-sintered, and a large number of large pores, which facilitate gas transport, are also visible in the LSTN-YSZ skeleton layer.

## 4 Conclusion

We employed the impregnation method to construct LSTN-YSZ(GDC) composite anodes innovatively and investigated the phase structure changes of the materials before and after impregnation. A SOFC with the configuration LSTN-YSZ (GDC) || YSZ || LSM-YSZ was developed. Electrochemical performance characterization revealed that at 800 °C and OCV, the polarization resistance of the cells after three impregnation cycles was 1.26 Ω cm<sup>2</sup>, representing a 50.9% reduction in polarization resistance compared to the untreated cells. Similarly, the ohmic resistance was reduced to varying degrees, and the maximum power density increased by 28.4%. Performance tests conducted at various temperatures and reduction time demonstrated that both polarization and ohmic resistance exhibited a trend of decreasing resistance, leading to improved cell performance with an increasing number of impregnations. The morphology of the nano-GDC anchored on the LSTN-YSZ skeleton was observed, suggesting that LSTN-YSZ (GDC) has potential as a composite anode for SOFC applications.

## Author contributions

The manuscript is shared by all authors and the final version of the manuscript is agreed upon.

## Acknowledgements

The authors greatly appreciate the support provided by Sichuan Science and Technology Program (under agreements No. 2021YFH0092, 2019YFH0177 and 2024YFHZ0038) and and Sichuan University of Science and Engineering (No. CX2024005 and No. CX2024007).

## References

1. Akin I, Li M, Lu Z, Sinclair DC: Oxygen-loss in A-site deficient Sr<sub>0.85</sub>La<sub>0.10</sub>TiO<sub>3</sub> perovskite. *RSC Adv.* **4**(61), 32549-32554 (2014).
2. Zhong F, Wang L, Fang H, Luo Y, Chen C, Lin L, Chen K, Jiang L: Cation-deficient perovskite Sr<sub>1-x</sub>Ti<sub>1-y</sub>Ni<sub>y</sub>O<sub>3-δ</sub> anodes with in-situ exsolution of Ni nanoparticles for direct ammonia solid oxide fuel cells. *Chem Eng J.* **471**, 144650 (2023).
3. Ma JJ, Li MQ, Jiang Y, Li CY, Tan H, Cheng JQ, Liu Y, Meng JJ, Chen YJ, Jiang CR: Tailoring A-site deficiency to synthesize nano-titanate with high conductivities and improved sintering characteristics. *Inorg Chem Commun.* **169**, 113017 (2024).
4. Jiang Y, Li CY, Huang HN, Zhang LX, Zhang JY, Jiang CR, Chen YJ, Yao YL, Ma JJ: A-site-deficiency range identified for in situ exsolution from (La<sub>0.4</sub>Sr<sub>0.6</sub>)<sub>1-α</sub>Ti<sub>0.95</sub>Ni<sub>0.05</sub>O<sub>3-δ</sub> electrodes for SOFC and SOEC. *Nanoscale.* **16**(32), 15396-15404 (2024).
5. Park BH, Choi GM: Electrochemical performance and stability of La<sub>0.2</sub>Sr<sub>0.8</sub>Ti<sub>0.9</sub>Ni<sub>0.1</sub>O<sub>3-δ</sub> and La<sub>0.2</sub>Sr<sub>0.8</sub>Ti<sub>0.9</sub>Ni<sub>0.1</sub>O<sub>3-δ</sub> - Gd<sub>0.2</sub>Ce<sub>0.8</sub>O<sub>2-δ</sub> anode with anode interlayer in H<sub>2</sub> and CH<sub>4</sub>. *Electrochim Acta.* **182**, 39-46 (2015).
6. Fan LQ, Xiong YP, Liu LB, Wang YW, Kishimoto H, Yamaji K, Horita T: Performance of Gd<sub>0.2</sub>Ce<sub>0.8</sub>O<sub>1.9</sub> infiltrated La<sub>0.2</sub>Sr<sub>0.8</sub>TiO<sub>3</sub> nanofiber scaffolds as anodes for solid oxide fuel cells. *J Power Sources.* **265**, 125-131 (2014).
7. Connor PA, Yue X, Savaniu CD, Price R, Triantafyllou G, Cassidy M, Kerherve G, Payne DJ, Maher RC, Cohen LF, Tomov RI, Glowacki BA, Kumar RV, Irvine JTS: Tailoring SOFC Electrode Microstructures for Improved

Performance. *Adv Energy Mater.* **8**(23), 1800120 (2018).

8. Jiang SP: A review of wet impregnation—An alternative method for the fabrication of high performance and nano-structured electrodes of solid oxide fuel cells. *Materials Science and Engineering: A.* **418**(1-2), 199-210 (2006).
9. Spiridigliozzi L, Di Bartolomeo E, Dell' Agli G, Zurlo F: GDC-Based Infiltrated Electrodes for Solid Oxide Electrolyzer Cells (SOECs). *Appl Sci.* **10**(11), 3882 (2020).
10. Lu L, Ni C, Cassidy M, Irvine JTS: Demonstration of high performance in a perovskite oxide supported solid oxide fuel cell based on La and Ca co-doped SrTiO<sub>3</sub>. *J Mater Chem A.* **4**(30), 11708-11718 (2016).
11. Huang Q-A, Hui R, Wang B, Zhang J: A review of AC impedance modeling and validation in SOFC diagnosis. *Electrochim Acta.* **52**(28), 8144-8164 (2007).

**Open Access** This chapter is licensed under the terms of the Creative Commons Attribution-NonCommercial 4.0 International License (<http://creativecommons.org/licenses/by-nc/4.0/>), which permits any noncommercial use, sharing, adaptation, distribution and reproduction in any medium or format, as long as you give appropriate credit to the original author(s) and the source, provide a link to the Creative Commons license and indicate if changes were made.

The images or other third party material in this chapter are included in the chapter's Creative Commons license, unless indicated otherwise in a credit line to the material. If material is not included in the chapter's Creative Commons license and your intended use is not permitted by statutory regulation or exceeds the permitted use, you will need to obtain permission directly from the copyright holder.

